Basal Autophagy Deficiency Causes Thyroid Follicular Epithelial Cell Death in Mice

Tomomi Kurashige[1], Yasuyo Nakajima[2], Mika Shimamura[1], Mutsumi Matsuyama[3], Masanobu Yamada[2], Masahiro Nakashima[3], Yuji Nagayama[1]

[1] Department of Molecular Medicine, Atomic Bomb Disease Institute, Nagasaki University, Nagasaki, 852-8523, Japan; [2] Department of Internal Medicine, Division of Endocrinology and Metabolism, Gunma University Graduate School of Medicine, Maebashi, 371-8511, Japan; [3] Department of Tumor and Diagnostic Pathology, Atomic Bomb Disease Institute, Nagasaki University, Nagasaki, 852-8523, Japan

ORCID numbers: 0000-0002-5216-5785 (T. Kurashige); 0000-0003-2630-2579 (Y. Nakashima); 0000-0002-3830-2173 (M. Shimamura); 0000-0003-2106-4436 (M. Matsuyama); 0000-0003-4426-2670 (M. Yamada); 0000-0002-9036-8735 (M. Nakashima); 0000-0002-5058-9349 (Y. Nagayama).

Correspondence/reprint request; Yuji Nagayama, MD/PhD, Department of Molecular Medicine, Atomic Bomb Disease Institute, Nagasaki University, 1-12-4 Sakamoto, Nagasaki 852-8523 Japan
TEL: +81-95- 819-7173, FAX: +81-95-819-7175, E-MAIL: nagayama@nagasaki-u.ac.jp

Key words: thyrocyte, autophagy, atg5, knockout, apoptosis

Disclosure: The authors also declare no conflict of interest.

Abbreviations: 53BP1, p53-binding protein 1; H&E, hematoxylin eosin; LC3, microtubule-associated protein 1 light chain 3; 8-OHdG, 8-hydroxy-2'-deoxyguanosine; KO, knockout; OD, optical density; PE, phosphatidylethanolamine; ROS, reactive oxygen species; thyrocye, thyroid follicular epithelial cell; TUNEL, terminal deoxynucleotidyl transferase (TdT)-mediated dUTP nick end-labeling; wt, wild type.

Abstract

Autophagy is a catabolic process that involves the degradation of cellular components through the lysosomal machinery, re-locating nutrients from unnecessary processes to more pivotal processes required for survival. It has been reported that systemic disruption of *Atg5* or *7* gene, a component of autophagy, is lethal, and that its tissue-specific disruption causes tissue degeneration in several organs. However, the functional significance of autophagy in the thyroid glands remained unknown. Our preliminary data imply the possible involvement of dysfunctional autophagy in radiation-induced thyroid carcinogenesis. Therefore, we evaluated the effect of *Atg5* gene knockout on the thyroid morphology and function. To this end, $Atg5^{flox/flox}$ mice were crossed with *TPO-Cre* mice, yielding the thyroid follicular epithelial cell (thyrocyte)-specific ATG5 deficient mic ($Atg5^{thyr\text{-}KO/KO}$). *Atg5* gene knockout was confirmed by a lack of ATG5 expression, and disruption of autophagy was demonstrated by a decrease in LC3-II puncta and an increase in p62. $Atg5^{thyr\text{-}KO/KO}$ mice were born normally, and thyroid morphology, thyroid weights, and serum T_4 and TSH levels were almost normal at 4 months. However, at 8 and 12 months, although thyroid function was still normal, a decrease in the number of thyrocytes, and an increase in $TUNEL^{+}$-thyrocytes *(i.e.*, apoptotic cells) were observed in $Atg5^{thyr\text{-}KO/KO}$ mice. Number of irregularly shaped follicles (gourd-shaped) was also increased. Excess oxidative stress was indicated by increased 8-OHdG and 53BP1 foci in $Atg5^{thyr\text{-}KO/KO}$ mice. These data demonstrate that thyrocytes gradually undergo degradation/cell death in the absence of basal levels of autophagy, indicating that autophagy is critical for the quality control of thyrocytes.

Introduction

Autophagy is a catabolic process that involves the degradation of cellular components through the lysosomal machinery, re-locating nutrients from unnecessary processes to more pivotal processes required for survival. This mechanism plays a role in not only the preservation of nutrients under starvation condition or other cellular stresses but also the normal turnover of cytoplasmic components. Using genetically engineering mice, disruption of autophagy has recently been shown to be important for maintaining the quality of proteins and organelles, and thus cellular homeostasis. Systemic disruption of *Atg5* or *Atg7* gene, encoding critical components for autophagy, causes neonatal death (1,2), and that their tissue-specific disruption induces tissue degeneration in neuron, liver, heart and pancreatic β-cells (1,3-6).

However, there are only a few studies reporting the functional significance of autophagy in the pathophysiology of the thyroid glands. For example, cytokine/iodine-mediated suppression of autophagy has been described in the thyroids of Hashimoto's thyroiditis (7-9). Modulation of autophagic activity has begun to be used for cancer treatment (see (10) for a review). Furthermore, our preliminary data imply the possible involvement of dysfunction of autophagy in radiation-induced thyroid carcinogenesis in young rats (11). However, as far as we know, the physiological significance of autophagy in the thyroid function and morphology remained totally unknown. Therefore, we generated the thyroid-specific *Atg5* knockout mice by crossing $Atg5^{flox/flox}$ and *TPO-Cre* mice, and evaluated the consequence of disruption of autophagy on the thyroid morphology and function.

Materials and methods

Mice used

$Atg5^{flox}$ mice, in which exon 3 of the *Atg5* gene was flanked by two *lox*P sequences, were originally generated by N. Mizushima (4) and provided by RIKEN Bioresource Center, Japan (http://en.brc.riken.jp/). TPO-Cre mice expressing Cre recombinase under the control of thyroglobulin promoter was previously obtained from S. Kimura in NIH (12). $Atg5^{flox/flox}$;*TPO-Cre*

mice (hereafter designated as *Atg5*$^{thyr\text{-}KO/KO}$, indicating thyroid-specific *Atg5* gene KO) were generated by crossing these two mice. In *Atg5*$^{thyr\text{-}KO}$ mice, Cre is expressed in thyrocytes after embryonic day 14 (E14), resulting in the deletion of the *lox*P-flanked exon 3. Controls include littermates of *Atg5*$^{thyr\text{-}KO/+}$ and *Atg5*$^{+/+}$ mice, because only a small amount of Atg5 is needed for autophagy (13).

All mice were kept in a specific pathogen free facility. Animal care and all experimental procedures were performed in accordance with the Guideline for Animal Experimentation of Nagasaki University with approval of the Institutional Animal Care and Use Committee (Permission number: 1309021089). All surgeries were performed under isoflurane anesthesia and all efforts were made to minimize suffering.

Experimental designs

At 4, 8 and 12 months, mice were anesthetized with isoflurane, from which bloods were collected via cardiac tap for serum preparation, and then euthanized by cervical dislocation. The thyroids were removed for histological examinations, and bloods were used to measure TSH and T_4 concentrations. Each group contained 3 to 4 mice of both sexes.

H&E staining and immunohistochemistry

The thyroids were fixed in 10% neutral-buffered formalin or Bouin's solution (023-17361, FUJIFILM Wako, Osaka, Japan, for 8-OHdG) and then embedded in paraffin. Four-μm-thick sections were prepared and H&E-stained or immunostained. The primary and secondary antibodies used were (i) rabbit monoclonal anti-ATG5 (14) and swine anti-rabbit IgG/HRP (15) for ATG5, (ii) guinea pig polyclonal anti-p62 (16) and Alexa Fluor 488-conjugated goat polyclonal anti-guinea pig IgG (17) for p62, (iii) rabbit polyclonal anti-LC3 (18) and Alexa Fluor 488-conjugated goat polyclonal anti-rabbit IgG (19) for LC3, (iv) rabbit polyclonal anti-ubiquitin (20) and Alexa Fluor 488-conjugated goat polyclonal anti-rabbit IgG (19) for ubiquitin, (v) rabbit anti-53BP1 (21) and Alexa Fluor 488-conjugated goat polyclonal anti-rabbit IgG (19) for 53BP1 and (vi) mouse monoclonal anti 8-OHdG (22) and Alexa Fluor 488-conjugated goat polyclonal

anti-mouse IgG (23) for 8-OHdG. The staining without the primary antibodies was performed as negative controls in all experiments. For HRP, color was developed with 3, 3'-diaminobenzidine (DAB) substrate. For, immunofluorescence, the slides were analyzed using an All-in-One BZ-9000 Fluorescence Microscope (Keyence, Osaka, Japan) and the fluorescent intensity was quantified using a BZ-II Analyzer (KEYENCE). 100 cells were evaluated in each sample to measure the fluorescent intensities of p62, ubiquitin and 8-OHdG, and number of LC3 puncta and 53BP1 foci.

Western blotting

Expression of LC3 and p62 was also determined by immunoblotting with 40 μg of thyroid tissues lysate prepared with RIPA buffer from *Atg5*$^{thyr\text{-}KO/KO}$ and *Atg5*$^{thyr\text{-}+/+}$ mice. Protein samples were resolved by sodium dodecyl sulfate polyacrylamide gel electrophoresis and transferred onto a polyvinylidene fluoride membrane (Bio-Rad Laboratories Inc., Tokyo, Japan). After blocking and incubation with an appropriate primary antibody, the antigen–antibody complexes were visualized using a horseradish peroxidase–conjugated secondary antibody and a chemiluminescence system (Thermo Fisher Scientific, Rockford, IL, U.S.). Detection was performed using a LAS-3000 imaging system (FUJIFILM Corporation, Tokyo, Japan). The primary and secondary antibodies used were (i) polyclonal rabbit anti-LC3 (18) and polyclonal goat anti-rabbit HRP-conjugated IgG (24) for LC3, (ii) polyclonal guinea pig anti-p62 (16) and polyclonal rabbit anti guinea pig HRP-conjugated IgG (25) for p62, and (iii) monoclonal mouse anti β-actin (26) and polyclonal horse anti-mouse HRP-conjugated IgG (27) for β–actin;.

Evaluation of apoptosis

TUNEL staining was performed with the Apop-tag™ Fluorescein Direct in situ apoptosis detection kit (Merck Millipore, Darmstadt, Germany). The slides were embedded with VECTASHIELD Mounting Medium containing DAPI (Vector Laboratories, Burlingame, CA) and analyzed using an All-in-One BZ-9000 Fluorescence Microscope. 150 cells were evaluated in each sample to determine the percentages of TUNEL-positive cells. .

Serum TSH and T_4 measurements

Serum TSH was measured by specific mouse TSH RIA with mouse TSH/LH reference (AFP9090D), mouse TSH antiserum (AFP98991) (28) and rat TSH antigen (NIDDK-rTSH-I-9) as described previously (29,30). Serum T_4 was measured with Mouse T4/Thyroxine ELISA Kit (LS-F10014, LifeSpan BioSciences, WA, USA) with the OD value of each well determined using a microplate reader (2030 Multilabel Plate Reader ARVO X3, PerkinElmer, Branchburg, NJ, USA) set to 450 nm.

Evaluation of thyroid morphology

The detailed analyses of thyroid morphology were performed according to the previously published methods (31-33). Sections of the whole thyroid gland at x400 magnification were used to assess the area of the follicles. The inner area of the thyroid gland at half the maximum length in the longitudinal places considered the central zone, and the area surrounding the central zone was considered the peripheral zone. The number of nuclei was counted in each area, and the values were converted to the values per 1,000 μm^2.

Statistical analyses

All data are expressed as mean $\pm$ S.E. and differences between groups were examined for statistical significance using the Dunnett's test. A p-value of less than 0.05 was considered statistically significant.

Results

In autophagy, cellular organelles, lipids, proteins and also invading microbes are sequestered in autophagosomes and are eventually fused with lysosome for degradation. In its initial steps, the soluble form of LC3-I (the mammalian homologue of yeast ATG8) is conjugated to PE resulting in formation of LC3-II, which is then associated with autophagosomal membrane, and forms autophagosome. Thus, the amount of LC3-II is an indicative of autophagy flux. This can be

monitored by western blotting showing the presence of a LC3-II band in addition to a LC3-I band or immunohistochemical analysis showing alteration of LC3 staining pattern from diffuse to punctate appearance (34). Furthermore, p62, a substrate of autophagy, is degraded in lysosome in the final step of autophagy (35). Thus, it is important to show both an increase in LC3-II/LC3 puncta and a decrease in p62 to confirm the complete process of autophagy (34,36).

In the thyroid glands of the wt mice, LC3 puncta were sparely observed and low expression levels of p62 were detectable in immune fluorescence analysis, and faint LC3-II band but no p62 band was detectable in western blot analysis (Fig. 1), indicating the low levels of autophagy in the thyroid cells in the steady state. Next, thyroid-specific knockout mice of ATG5 (*Atg5*$^{thyr\text{-}KO/KO}$ mice) were generated by crossing *Atg5*$^{flox/flox}$ and *TPO-Cre* mice. Absence of ATG5 protein expression and of LC3 puncta, and accumulation of p62 confirmed successful deletion of *Atg5* gene (Fig. 1). All the differences were confirmed by quantification (Fig. 1). *Atg5*$^{thyr\text{-}KO/KO}$ mice were born normally at an expected Mendelian frequency. The thyroid weights (data not shown), the ratios of thyroid to body weights, and serum concentrations of T_4 and TSH were all normal in 4-, 8- and 12-month-old *Atg5*$^{thyr\text{-}KO/KO}$ mice, with an exception of a slight increase in TSH in *Atg5*$^{thyr\text{-}KO/KO}$ mice compared with the wt mice at 4 months (Fig. 2), implying very mild hypothyroidism. Lower TSH in females than males at 4 months has previously been reported (37).

In H&E staining of the thyroid glands (Fig. 3), although the thyroid morphology was normal in 4-month-old *Atg5*$^{thyr\text{-}KO/KO}$ mice, the thinning of thyrocytes gradually appeared in 8- and 12-month-old *Atg5*$^{thyr\text{-}KO/KO}$ mice as compared to the wt mice. In the detailed analysis of thyroid morphological alterations (31-33), the thinning of thyrocytes were confirmed by measuring the epithelial height (Fig. 4A), and likely attributed to a decreased number of follicular epithelial cells. Thus, although the follicular sizes were similar between the wt and *Atg5*$^{thyr\text{-}KO/KO}$ mice (except 8- and 12-month-old male mice) (Fig. 4B), number of nuclei (*i.e.*, number of thyrocytes) per unit area were lower in *Atg5*$^{thyr\text{-}KO/KO}$ mice than the wt mice (Fig. 4C). Another interesting finding was appearance of irregularly shaped follicles. Thus, number of the gourd-shaped follicles was increased in 8- and 12-month-old *Atg5*$^{thyr\text{-}KO/KO}$ mice *versus* the wt mice (Fig. 4D).

In immunohistochemical staining, TUNEL was performed to see if decreased number of the

thyrocytes was due to apoptosis. Indeed TUNEL-thyrocytes were gradually increased in 8- and 12-month-old *Atg5*$^{thyr\text{-}KO/KO}$ mice (Figs. 5A and 6). Increased ubiquitin staining, a marker for accumulation and aggregation of misfolded proteins, was already observed in 4-month-old *Atg5*$^{thyr\text{-}KO/KO}$ mice, and gradually exacerbated in the 12-month experimental period (Fig. 5B and 6).

Because it has been reported that autophagy controls intracellular ROS levels (38), ROS-induced genomic damages were evaluated by using 53BP1 and 8-OHdG as markers. 53BP1 accumulates at the DNA double strand break sites (39), and 8-OHdG is a oxidized nucleotide guanine (40) and an indicator of oxidative stress (41). As shown in Figs. 5C & D and 6, the fluorescence intensity of 8-OHdG, not 53BP1, staining was higher in *Atg5*$^{thyr\text{-}KO/KO}$ mice than wt mice at 4 months. Because 8-OHdG is more sensitive than 53BP1 for detecting ROS-induced DNA damages (42), these data suggest a mild increase in oxidative stress in thyrocytes lacking autophagy. At 8 and 12 months, number of 53BP1 foci was also elevated, albeit very low levels, in *Atg5*$^{thyr\text{-}KO/KO}$ mice, demonstrating higher ROS production in the later period. Of interest, this fluorescence intensity of 8-OHdG staining was more intense in males than in females in both *Atg5*$^{thyr\text{-}KO/KO}$ mice and wt mice.

Discussion

We here studied the long-term effect of autophagy defect in the thyroids of mice, and found for the first time gradual degeneration and eventual cell death of thyrocytes. In 4-month-old *Atg5*$^{thyr\text{-}KO/KO}$ mice, although the thyroids are apparently normal in H&E staining, accumulation of misfolded proteins could already be detected by immunohistochemical staining with anti-ubiquitin antibody. Cytoplasmic accumulation of (poly)ubiquitinated proteins is a widely accepted to be a hallmark of protein accumulation by autophagy deficiency (1,3,4), which, for an example, can be seen soon (4 days) after deletion of *Atg5* gene in liver, from which cytoplasmic inclusion bodies were gradually developed (4). Increased ubiquitinated protein indicates accumulation of polyubiquitinated proteins targeted to autophagosomes by p62. Then accumulation of aggregated proteins likely lead eventually to thyrocyte death as evidenced by a decrease in thyrocyte number and an increase in apoptotic thyrocytes, although thyroid function was still within normal ranges in

even 12-month-old *Atg5*$^{thyr\text{-}KO/KO}$ mice. Of interest, the cell death resulted in the thinning of thyrocytes. Width of thyrocyte is usually an indicator for cell function, but, in our study, the thinning seems to be rather due to the elongation of the remaining surviving thyrocytes. We also prefer to presume that the gourd-like follicles might have arisen from the fusion of follicles; the reduced numbers of thyrocytes cannot keep follicle structure.

Since it has recently been reported that the components of autophagy have various non-autophagic functions such as endocytosis and exocytosis (43), another interpretation for thinning of thyrocytes is that an defect in membrane transport increased colloid accumulation which led to the appearance of thinning of the follicular layer. This issue should be clarified in the future.

The similar results have previously been reported; for example, neuronal degeneration characterized by growth retardation and progressive motor and behavioral deficits early in life in neural cell-specific *Atg5* or *Atg7* KO mice (3,4), cardiomyopathy in cardiocyte-specific *Atg5* KO mice (5), progressive degeneration, impaired insulin secretion (due to lower ATP production) and reduced proliferation in response to high-fat-diet, an autophagy inducer, in β-cells in β-cell-specific *Atg7* KO mice (6,44), and liver cell damage and death in hepatocyte-targeted *Atg7* KO mice (1).

We also found increased 8-OHdG at 4 months and increased 8-OHdG and 53BP1 at 8 and 12 months in *Atg5*$^{thyr\text{-}KO/KO}$ mice. Oxidative stress burdens have been demonstrated to be elevated in autophagy-deficient cells; abnormal mitochondria can be a source of ROS (45), and protein re-folding in the endoplasmic reticulum by protein disulphide isomerases can also elevate ROS through redox reactions involving free radicals (46). However, higher oxidative stress in both the wt and *Atg5*$^{thyr\text{-}KO/KO}$ male mice than female mice but the similar levels of thyrocyte death between male and female mice suggest that excess oxidative stress is unlikely to be another reason for degradation of thyrocytes observed in the present study. This sex disparity is in line with previous reports showing higher anti-oxidative stress defense in female mice (47-49). On the other hand, it has been reported that the thyroid glands of female rats are exposed to higher oxidative stress due to increased ROS production by NOX4 and decreased ROS degradation (50).

Our results altogether support a pro-survival role for autophagy in sustaining energy homeostasis and maintaining protein and organelle quality control by eliminating damaged proteins and

organelles at the basal levels in thyrocytes. Thus, the critical role of basal autophagic activity in thyrocyte homeostasis should be emphasized. Furthermore, induced autophagy may also be crucial for eliminating unnecessary and harmful proteins/damaged organelles and possibly other cellular stresses, thus avoiding cell degeneration/death.

In addition, association of autophagy and cancer development has also been proposed (10). Indeed, it has been demonstrated that liver tumors developed in mosaically *Atg5* or *Atg7* deficient mice by 6 to 9 months (51,52). Impaired DNA damage response has been demonstrated in autophagy-deficient cells (53,54), which, in addition to excess oxidative stress, may be a cause of carcinogenesis. By contrast, we could not observe any abnormally proliferative legions in the thyroids of $Atg5^{thyr\text{-}KO/KO}$ mice during a 12-month experimental course in this study. Future studies will be necessary to elucidate the relationship between autophagy and thyroid carcinogenesis.

Acknowledgements

This study was in part supported by the Japan Society for the Promotion of Science (KAKENHI Grant No. 16K00548 for TK) and by a Joint Research Grant from the Network-type Joint Usage/Research Center for Radiation Disaster Medical Science of Hiroshima University, Nagasaki University and Fukushima Medical University.

Author Disclosure Statement

The authors have no potential conflict of interest to declare.

References

1. Komatsu M, Waguri S, Ueno T, Iwata J, Murata S, Tanida I, Ezaki J, Mizushima N, Ohsumi Y, Uchiyama Y, Kominami E, Tanaka K, Chiba T. Impairment of starvation-induced and constitutive autophagy in Atg7-deficient mice. *J Cell Biol.* 2005;**169**(3):425-434.

2. Kuma A, Hatano M, Matsui M, Yamamoto A, Nakaya H, Yoshimori T, Ohsumi Y, Tokuhisa T, Mizushima N. The role of autophagy during the early neonatal starvation period. *Nature.* 2004;**432**(7020):1032-1036.

3. Komatsu M, Waguri S, Chiba T, Murata S, Iwata J, Tanida I, Ueno T, Koike M, Uchiyama Y, Kominami E, Tanaka K. Loss of autophagy in the central nervous system causes neurodegeneration in mice. *Nature.* 2006;**441**(7095):880-884.

4. Hara T, Nakamura K, Matsui M, Yamamoto A, Nakahara Y, Suzuki-Migishima R, Yokoyama M, Mishima K, Saito I, Okano H, Mizushima N. Suppression of basal autophagy in neural cells causes neurodegenerative disease in mice. *Nature.* 2006;**441**(7095):885-889.

5. Nakai A, Yamaguchi O, Takeda T, Higuchi Y, Hikoso S, Taniike M, Omiya S, Mizote I, Matsumura Y, Asahi M, Nishida K, Hori M, Mizushima N, Otsu K. The role of autophagy in cardiomyocytes in the basal state and in response to hemodynamic stress. *Nat Med.* 2007;**13**(5):619-624.

6. Ebato C, Uchida T, Arakawa M, Komatsu M, Ueno T, Komiya K, Azuma K, Hirose T, Tanaka K, Kominami E, Kawamori R, Fujitani Y, Watada H. Autophagy is important in islet homeostasis and compensatory increase of beta cell mass in response to high-fat diet. *Cell Metab.* 2008;**8**(4):325-332.

7. Lu Q, Luo X, Mao C, Zheng T, Liu B, Dong X, Zhou Y, Xu C, Mou X, Wu F, Bu L, Yuan G. Caveolin-1 regulates autophagy activity in thyroid follicular cells and is involved in Hashimoto's thyroiditis disease. *Endocr J.* 2018;**65**(9):893-901.

8. Zheng T, Xu C, Mao C, Mou X, Wu F, Wang X, Bu L, Zhou Y, Luo X, Lu Q, Liu H, Yuan G, Wang S, Chen D, Xiao Y. Increased Interleukin-23 in Hashimoto's Thyroiditis Disease Induces Autophagy Suppression and Reactive Oxygen Species Accumulation. *Front*

Immunol. 2018;**9**:96.

9. Xu C, Wu F, Mao C, Wang X, Zheng T, Bu L, Mou X, Zhou Y, Yuan G, Wang S, Xiao Y. Excess iodine promotes apoptosis of thyroid follicular epithelial cells by inducing autophagy suppression and is associated with Hashimoto thyroiditis disease. *J Autoimmun.* 2016;**75**:50-57.

10. Netea-Maier RT, Kluck V, Plantinga TS, Smit JW. Autophagy in thyroid cancer: present knowledge and future perspectives. *Front Endocrinol*. 2015;**6**:22.

11. Matsuu-Matsuyama M, Shichijo K, Okaichi K, Kurashige T, Kondo H, Miura S, Nakashima M. Effect of age on the sensitivity of the rat thyroid gland to ionizing radiation. *J Radiat Res.* 2015;**56**(3):493-501.

12. Kusakabe T, Kawaguchi A, Kawaguchi R, Feigenbaum L, Kimura S. Thyrocyte-specific expression of Cre recombinase in transgenic mice. *Genesis.* 2004;**39**(3):212-216.

13. Hosokawa N, Hara Y, Mizushima N. Generation of cell lines with tetracycline-regulated autophagy and a role for autophagy in controlling cell size. *FEBS lett.* 2007;**581**(15):2623-2629.

14. RRID:AB_2650499, http://scicrunch.org/resolver/AB_2650499.

15. RRID:AB_2617141, http://scicrunch.org/resolver/AB_2617141.

16. RRID:AB_2687531, http://scicrunch.org/resolver/AB_2687531.

17. RRID:AB_2736871, http://scicrunch.org/resolver/AB_2736871.

18. RRID:AB_2274121, http://scicrunch.org/resolver/AB_2274121.

19. RRID:AB_143165, http://scicrunch.org/resolver/AB_143165.

20. RRID:AB_2039666, http://scicrunch.org/resolver/AB_2039666.

21. RRID:AB_185520, http://scicrunch.org/resolver/AB_185520.

22. RRID:AB_1106819, http://scicrunch.org/resolver/AB_1106819.

23. RRID:AB_2534069, http://scicrunch.org/resolver/AB_2534069.

24. RRID:AB_2099233, http://scicrunch.org/resolver/AB_2099233.

25. RRID:AB_88247, http://scicrunch.org/resolver/AB_88247.

26. RRID:AB_2714189, http://scicrunch.org/resolver/AB_2714189.

27. RRID:AB_330924, http://scicrunch.org/resolver/AB_330924.

28. RRID:AB_2810234, http://scicrunch.org/resolver/AB_2810234.

29. Shimamura M, Nakahara M, Orim F, Kurashige T, Mitsutake N, Nakashima M, Kondo S, Yamada M, Taguchi R, Kimura S, Nagayama Y. Postnatal expression of BRAFV600E does not induce thyroid cancer in mouse models of thyroid papillary carcinoma. *Endocrinology.* 2013;**154**(11):4423-4430.

30. Shibusawa N, Yamada M, Hirato J, Monden T, Satoh T, Mori M. Requirement of thyrotropin-releasing hormone for the postnatal functions of pituitary thyrotrophs: ontogeny study of congenital tertiary hypothyroidism in mice. *Mol endocrinol.* 2000;**14**(1):137-146.

31. Lee J, Yi S, Kang YE, Kim HW, Joung KH, Sul HJ, Kim KS, Shong M. Morphological and Functional Changes in the Thyroid Follicles of the Aged Murine and Humans. *J Pathol Transl Med.* 2016;**50**(6):426-435.

32. Bianco AC, Anderson G, Forrest D, Galton VA, Gereben B, Kim BW, Kopp PA, Liao XH, Obregon MJ, Peeters RP, Refetoff S, Sharlin DS, Simonides WS, Weiss RE, Williams GR. American Thyroid Association Guide to investigating thyroid hormone economy and action in rodent and cell models. *Thyroid.* 2014;**24**(1):88-168.

33. Wade MG, Parent S, Finnson KW, Foster W, Younglai E, McMahon A, Cyr DG, Hughes C. Thyroid toxicity due to subchronic exposure to a complex mixture of 16 organochlorines, lead, and cadmium. *Toxicol Sci.* 2002;**67**(2):207-218.

34. Klionsky DJ, Abeliovich H, Agostinis P, Agrawal DK, Aliev G, Askew DS, Baba M, Baehrecke EH, Bahr BA, Ballabio A, Bamber BA, Bassham DC, Bergamini E, Bi X, Biard-Piechaczyk M, Blum JS, Bredesen DE, Brodsky JL, Brumell JH, Brunk UT, Bursch W, Camougrand N, Cebollero E, Cecconi F, Chen Y, Chin LS, Choi A, Chu CT, Chung J, Clarke PG, Clark RS, Clarke SG, Clave C, Cleveland JL, Codogno P, Colombo MI, Coto-Montes A, Cregg JM, Cuervo AM, Debnath J, Demarchi F, Dennis PB, Dennis PA, Deretic V, Devenish RJ, Di Sano F, Dice JF, Difiglia M, Dinesh-Kumar S, Distelhorst CW, Djavaheri-Mergny M, Dorsey FC, Droge W, Dron M, Dunn WA, Jr., Duszenko M, Eissa NT, Elazar Z, Esclatine A, Eskelinen EL, Fesus L, Finley KD, Fuentes JM, Fueyo J, Fujisaki K,

Galliot B, Gao FB, Gewirtz DA, Gibson SB, Gohla A, Goldberg AL, Gonzalez R, Gonzalez-Estevez C, Gorski S, Gottlieb RA, Haussinger D, He YW, Heidenreich K, Hill JA, Hoyer-Hansen M, Hu X, Huang WP, Iwasaki A, Jaattela M, Jackson WT, Jiang X, Jin S, Johansen T, Jung JU, Kadowaki M, Kang C, Kelekar A, Kessel DH, Kiel JA, Kim HP, Kimchi A, Kinsella TJ, Kiselyov K, Kitamoto K, Knecht E, Komatsu M, Kominami E, Kondo S, Kovacs AL, Kroemer G, Kuan CY, Kumar R, Kundu M, Landry J, Laporte M, Le W, Lei HY, Lenardo MJ, Levine B, Lieberman A, Lim KL, Lin FC, Liou W, Liu LF, Lopez-Berestein G, Lopez-Otin C, Lu B, Macleod KF, Malorni W, Martinet W, Matsuoka K, Mautner J, Meijer AJ, Melendez A, Michels P, Miotto G, Mistiaen WP, Mizushima N, Mograbi B, Monastyrska I, Moore MN, Moreira PI, Moriyasu Y, Motyl T, Munz C, Murphy LO, Naqvi NI, Neufeld TP, Nishino I, Nixon RA, Noda T, Nurnberg B, Ogawa M, Oleinick NL, Olsen LJ, Ozpolat B, Paglin S, Palmer GE, Papassideri I, Parkes M, Perlmutter DH, Perry G, Piacentini M, Pinkas-Kramarski R, Prescott M, Proikas-Cezanne T, Raben N, Rami A, Reggiori F, Rohrer B, Rubinsztein DC, Ryan KM, Sadoshima J, Sakagami H, Sakai Y, Sandri M, Sasakawa C, Sass M, Schneider C, Seglen PO, Seleverstov O, Settleman J, Shacka JJ, Shapiro IM, Sibirny A, Silva-Zacarin EC, Simon HU, Simone C, Simonsen A, Smith MA, Spanel-Borowski K, Srinivas V, Steeves M, Stenmark H, Stromhaug PE, Subauste CS, Sugimoto S, Sulzer D, Suzuki T, Swanson MS, Tabas I, Takeshita F, Talbot NJ, Talloczy Z, Tanaka K, Tanaka K, Tanida I, Taylor GS, Taylor JP, Terman A, Tettamanti G, Thompson CB, Thumm M, Tolkovsky AM, Tooze SA, Truant R, Tumanovska LV, Uchiyama Y, Ueno T, Uzcategui NL, van der Klei I, Vaquero EC, Vellai T, Vogel MW, Wang HG, Webster P, Wiley JW, Xi Z, Xiao G, Yahalom J, Yang JM, Yap G, Yin XM, Yoshimori T, Yu L, Yue Z, Yuzaki M, Zabirnyk O, Zheng X, Zhu X, Deter RL. Guidelines for the use and interpretation of assays for monitoring autophagy in higher eukaryotes. *Autophagy.* 2008;**4**(2):151-175.

35. Bjorkoy G, Lamark T, Brech A, Outzen H, Perander M, Overvatn A, Stenmark H, Johansen T. p62/SQSTM1 forms protein aggregates degraded by autophagy and has a protective effect on huntingtin-induced cell death. *J Cell Biol.* 2005;**171**(4):603-614.

36. Yoshii SR, Mizushima N. Monitoring and Measuring Autophagy. *Int J MOl Sci.* 2017;**18**(9).E1865.

37. McLachlan SM, Hamidi S, Aliesky H, Williams RW, Rapoport B. Sex, genetics, and the control of thyroxine and thyrotropin in mice. *Thyroid* 2014;**24**(7):1080-1087.

38. Li L, Tan J, Miao Y, Lei P, Zhang Q. ROS and Autophagy: Interactions and Molecular Regulatory Mechanisms. *Cell Mol Neurobiol.* 2015;**35**(5):615-621.

39. Ward IM, Minn K, Jorda KG, Chen J. Accumulation of checkpoint protein 53BP1 at DNA breaks involves its binding to phosphorylated histone H2AX. *J Biol Chem.* 2003;**278**(22):19579-19582.

40. Kasai H, Hayami H, Yamaizumi Z, SaitoH, Nishimura S. Detection and identification of mutagens and carcinogens as their adducts with guanosine derivatives. *Nucl Acids Res.* 1984;**12**(4):2127-2136.

41. Cadet J, Douki T, Gasparutto D, Ravanat JL. Oxidative damage to DNA: formation, measurement and biochemical features. *Mut Res.* 2003;**531**(1-2):5-23.

42. Hall EJ, Giaccia AJ. Molecular mechanisms of DNA and chromosome damage and repair. *Radiobiology for the Radiologist, 7th edit Lippincott Williams & Wilkins.* 2012.

43. Galluzzi L, Green DR. Autophagy-Independent Functions of the Autophagy Machinery. *Cell.* 2019;**177**(7):1682-1699.

44. Fujitani Y, Ebato C, Uchida T, Kawamori R, Watada H. beta-cell autophagy: A novel mechanism regulating beta-cell function and mass: Lessons from beta-cell-specific Atg7-deficient mice. *Islets.* 2009;**1**(2):151-153.

45. Fariss MW, Chan CB, Patel M, Van Houten B, Orrenius S. Role of mitochondria in toxic oxidative stress. *Mol Interv.* 2005;**5**(2):94-111.

46. Tu BP, Weissman JS. Oxidative protein folding in eukaryotes: mechanisms and consequences. *J Cell Biol.* 2004;**164**(3):341-346.

47. Celestino I, Checconi P, Amatore D, De Angelis M, Coluccio P, Dattilo R, Alunni Fegatelli D, Clemente AM, Matarrese P, Torcia MG, Mancinelli R, Mammola CL, Garaci E, Vestri AR, Malorni W, Palamara AT, Nencioni L. Differential Redox State Contributes to Sex

Disparities in the Response to Influenza Virus Infection in Male and Female Mice. *Front Immunol.* 2018;**9**:1747.

48. Anezaki Y, Ohshima S, Ishii H, Kinoshita N, Dohmen T, Kataoka E, Sato W, Iizuka M, Goto T, Sasaki J, Sasaki T, Suzuki A, Ohnishi H, Horie Y. Sex difference in the liver of hepatocyte-specific Pten-deficient mice: A model of nonalcoholic steatohepatitis. *Hepatol Res.* 2009;**39**(6):609-618.

49. Ji H, Zheng W, Menini S, Pesce C, Kim J, Wu X, Mulroney SE, Sandberg K. Female protection in progressive renal disease is associated with estradiol attenuation of superoxide production. *Gend Med.* 2007;**4**(1):56-71.

50. Fortunato RS, Braga WM, Ortenzi VH, Rodrigues DC, Andrade BM, Miranda-Alves L, Rondinelli E, Dupuy C, Ferreira AC, Carvalho DP. Sexual dimorphism of thyroid reactive oxygen species production due to higher NADPH oxidase 4 expression in female thyroid glands. *Thyroid.* 2013;**23**(1):111-119.

51. Takamura A, Komatsu M, Hara T, Sakamoto A, Kishi C, Waguri S, Eishi Y, Hino O, Tanaka K, Mizushima N. Autophagy-deficient mice develop multiple liver tumors. *Genes Dev.* 2011;**25**(8):795-800.

52. Inami Y, Waguri S, Sakamoto A, Kouno T, Nakada K, Hino O, Watanabe S, Ando J, Iwadate M, Yamamoto M, Lee MS, Tanaka K, Komatsu M. Persistent activation of Nrf2 through p62 in hepatocellular carcinoma cells. *J Cell Biol.* 2011;**193**(2):275-284.

53. Xu F, Li X, Yan L, Yuan N, Fang Y, Cao Y, Xu L, Zhang X, Xu L, Ge C, An N, Jiang G, Xie J, Zhang H, Jiang J, Li X, Yao L, Zhang S, Zhou D, Wang J. Autophagy Promotes the Repair of Radiation-Induced DNA Damage in Bone Marrow Hematopoietic Cells via Enhanced STAT3 Signaling. *Radiat Res.* 2017;**187**(3):382-396.

54. Bae H, Guan JL. Suppression of autophagy by FIP200 deletion impairs DNA damage repair and increases cell death upon treatments with anticancer agents. *Mol Cancer Res.* 2011;**9**(9):1232-1241.

Figure legends

Fig. 1. Immunohistochemical staining and western blot analysis of the thyroid tissues from 4-month-old *Atg5*$^{+/+}$, *Atg5*$^{thyr\text{-}KO/+}$, *Atg5*$^{thyr\text{-}KO/KO}$ male mice for ATG5, p62 and LC3. Mice (n = 3) were sacrificed at 4 weeks of age. The thyroid glands were removed and subjected to immunohistochemical staining, western blotting and quantification of expression levels as described in the Materials and Methods. Note that quantification of ATG5 expression was performed using immunofluorescent staining of ATG5 (data not shown), although the pictures shown here are with HRP and DAB. Data are means $\pm$ S.E.. *, **, $p < 0.05$ and $p < 0.01$, respectively. The original magnifications, x400 for ATG5 and p62 and x1000 for LC3.

Fig.2. The thyroid weight/body weight ratios, and serum T_4 and TSH concentrations in 4-, 8- and 12-month-old control and *Atg5*$^{thyr\text{-}KO/KO}$ mice. The thyroid glands and bloods were obtained from 4-, 8- and 12-month-old mice (n = 3~4 for each group). T4 and TSH were measured as described in the Materials and Methods. The black and white bars indicate the control and *Atg5*$^{thyr\text{-}KO/KO}$ mice, respectively. Data are means $\pm$ S.E.. *, $p < 0.05$.

Fig. 3. H&E staining of the thyroid glands from 4-, 8- and 12-month-old control and *Atg5*$^{thyr\text{-}KO/KO}$ mice. The thyroid glands removed in Fig. 2 (n = 3~4 for each group) were subjected to H&E staining as described in the Materials and Methods. Because histology was essentially same between males and females, the representative photos of male mice were shown. Original magnification, x400.

Fig. 4. Measurements of epithelial height (A), follicular area (B), and numbers of nuclei/unit area (C) and gourd-shaped follicles (D). The thyroid glands removed in Fig. 2 (n = 3~4 for each group) were used for measurements. The black and white bars indicate the control and *Atg5*$^{thyr\text{-}KO/KO}$ mice, respectively. Diagram for measurement of epithelial height was shown in (A), where Lf and Lc means the lengths of follicle and colloid, and Wc and Wf the widths of follicle and colloid,

respectively (33). The representative photo for gourd-shaped follicles was shown in (D). Data are means ± S.E.. *, **, $p < 0.05$ and $p < 0.01$, respectively.

Fig. 5. Measurements of TUNEL-positive thyrocytes (A), fluorescence intensities of ubiquitin and 8-OHdG (B, C) and number of 53BP1 foci (D). The thyroid glands removed in Fig. 2 (n = 3~4 for each group) were used for staining and measurements. The black and white bars indicate the control and *Atg5*$^{thyr\text{-}KO/KO}$ mice, respectively. Data are means ± S.E.. *, **, $p < 0.05$ and $p < 0.01$, respectively, compared to the controls.

Fig. 6. Immunohistochemical staining of TUNEL, ubiquitin, 8-OHdG and 53BP1 in 4-, 8- and 12-month-old control and *Atg5*$^{thyr\text{-}KO/KO}$ mice. The thyroid glands obtained in Fig. 2 (n = 3~4 for each group) were used for staining. The original magnification, x400. The representative photos of male mice were shown for TUNEL, ubiquitin and 53BP1, because different results between males and females were only observed in 8-OHdG.

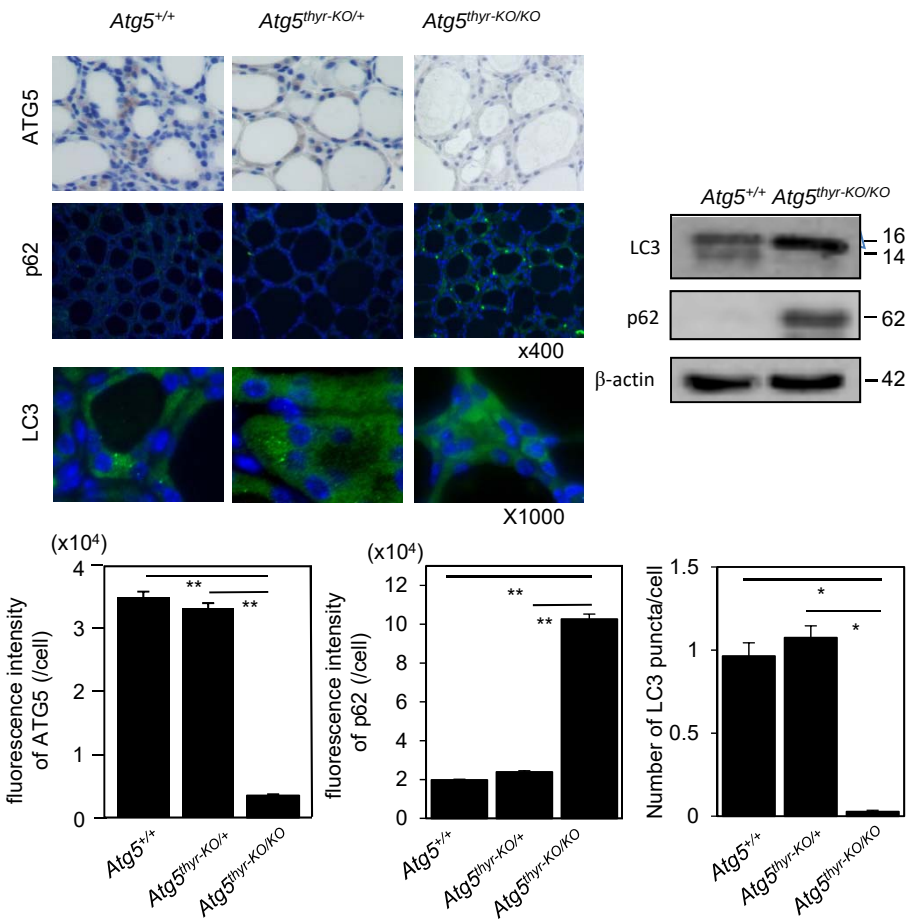

Kurashige et al. Figure 1

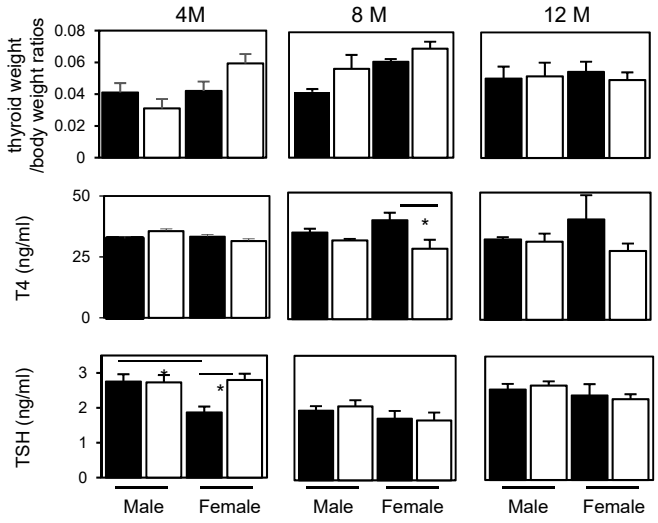

Kurashige et al. Figure 2

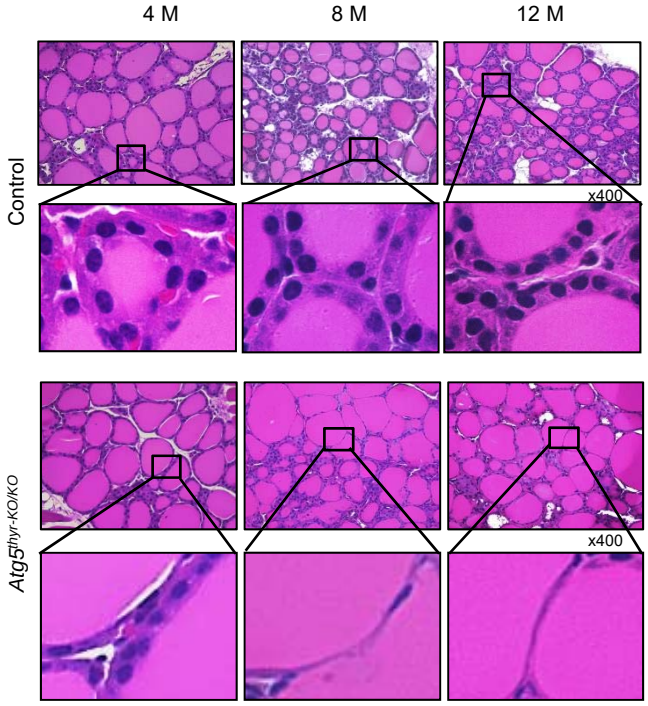

Kurashige et al. Figure 3

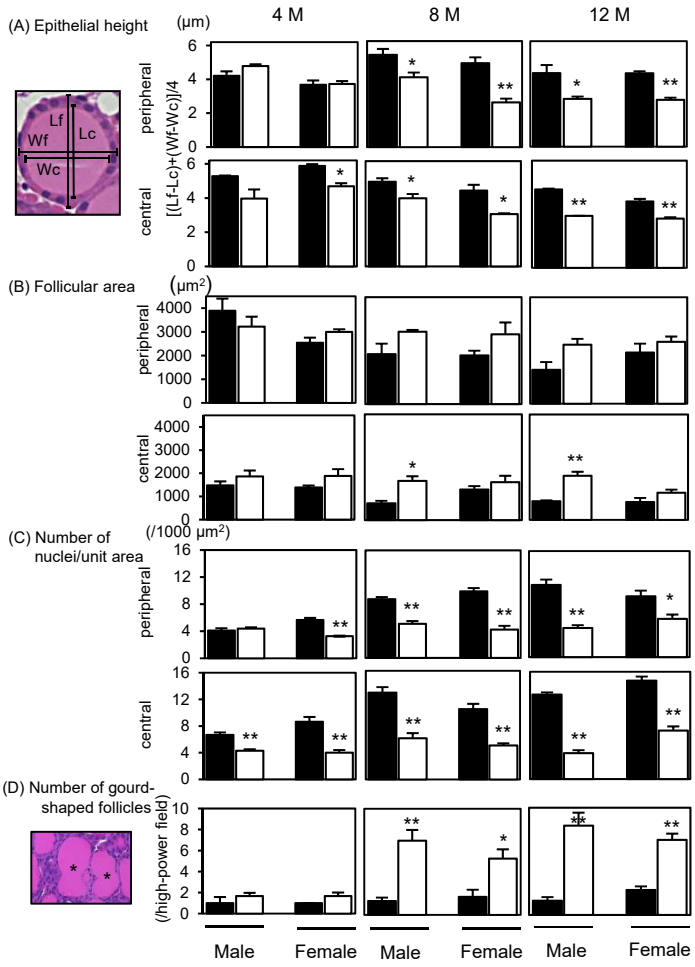

Kurashige et al. Figure 4

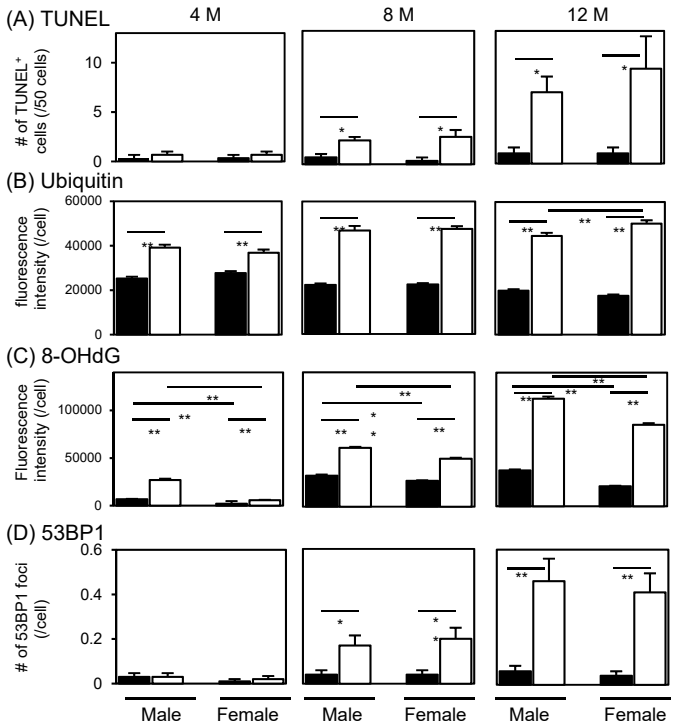

Kurashige et al. Figure 5

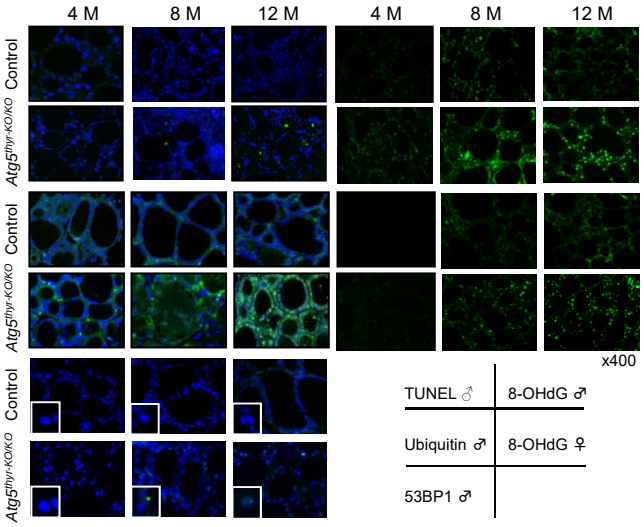

Kurashige et al. Figure 6